JOURNAL OF IMAGING SCIENCE AND TECHNOLOGY • Volume 43, Number 1, January/February 1999

Photoluminescent Quantum Clusters of γAgI and I_m^{n-} in Iodide-Doped AgCl Systems

S. H. Ehrlich[*,†]
Manufacturing Research and Engineering Organization, Eastman Kodak Company, Rochester, New York

J. Edwards
Imaging Research and Advanced Development, Eastman Kodak Company, Rochester, New York

---

The photoluminescent emission of AgCl dispersions doped with small concentrations of γAgI and I_m^{n-} clusters has been investigated. Heterogeneous γAgI phases exist within the cubic AgCl host lattice to provide enhanced photographic properties. The spatial correlation diagram involving recombination energy at peak photoluminescence wavelength for βAgI (wurtzite) and γ (sphalerite) AgI versus the silver iodide cluster diameter allowed the calculation of the γAgI incorporated cluster diameter within a cubic AgCl dispersion. The competition for the conduction band electron by the bound hole on the iodide sites with the dopant is noted by the quenching of the photoluminescence. The (LUMO) lowest unoccupied level of the iodide species is positioned very close to the bottom of the conduction band. The incorporation of 0.30 M% soluble KI or 4.30 M/V% at 93% of the crystal growth provides a maximum speed position and significant change in the spectral band profile correlating with the structures of γAgI. The I_m^{n-} clusters observed at longer wavelengths were assigned to 2 I_m^{n-} dimers that relate only indirectly to the photographic process.

Journal of Imaging Science and Technology 43: 15–29 (1999)

Introduction

Iodide ions in AgCl microcrystallites, even in the range of 10^{-7} to 10^{-4} mole fraction, often have energy states in the forbidden band gap and can modify the optical and electronic characteristics of the host crystals.[1] The low-temperature photoluminescence is also modified by the presence of iodide.[2–5] Moser, Ahrenkiel, and Lyn investigated AgCl crystals doped with small concentrations of AgI and were able to reveal discrete absorption and emission bands associated with iodide ions.[6a] The AgCl,I crystals were grown from the melt either by a Bridgman technique[6b] or as sheet crystals solidified between quartz plates.[6c] The narrow absorption band with intensity proportional to the iodide content could be resolved from the AgCl lattice absorption at low temperatures. Excitation in this (3.13 eV, 396.0 nm) band at low temperatures, 5 K, produces a distinct emission band peaking at 2.67 eV or 464.2 nm. The oscillator strength is found to be low, 4×10^{-3}, whereas the radiative lifetime is somewhat long (6.0 µsec). The optical absorption edge at 5 K of a pure AgCl crystal was shown at 3.26 eV, 380 nm. The oscillator strength of the AgCl:I band was calculated using the Smakula formula shown by Dexter[7] which relates the oscillator strength f_{if} to the number of centers N by

$$N\left(cm^3\right) = 8.7 \times 10^{16} \frac{n}{\left(n^2+2\right)^2} \frac{1}{f_{if}} \alpha_{\max}\left(\mathrm{cm}^{-1}\right) W_{½}(\mathrm{eV}), \tag{1}$$

where n is the index of refraction of the host lattice at a wavelength corresponding to the band maximum; $\alpha_{\max}$ is the absorption coefficient at the band maximum, and $W_{1/2}$ is the width of the band at half-maximum. Utilizing the values $n = 2$, $N = 10^{18}/\mathrm{cm}^3$, $\alpha_{\max} = 6\ \mathrm{cm}^{-1}$, and $W_{1/2} = 0.130$ eV, one obtains[6a] $f_{if} = 4 \times 10^{-3}$.

The nature of the localized energy states involved was inferred from the above measurements and the model proposed that the excited electronic states for absorption and emission are effective-mass states or Wannier type excitons resulting in a small overlap with a localized closed-shell ground state on the I^- ion. The iodide anion I^- is isoelectronic with the Xe atom. The ground state of that atom is a $5p^6$ electron configuration. The iodide anion configuration $^1S_0$ ($5p^6$) with excitation should yield transitions to ^1P ($5p^5 6s^1$) (LS coupling) excited states. This heavy ion I^- should be described by the J – L coupling scheme 3/2, 1/2 in J of the excited state.[‡,8] The S to P transition is parity allowed, and therefore the low oscillator strength is not due to a parity-forbidden transition.

Original manuscript received August 28, 1998

[*] IS&T Fellow

[†] Present address: 12 Courtenay Circle, Pittsford, New York, 14534

[‡] Two types of vector coupling are considered by spectroscopists, the (LS) and the (jj) coupling; the first takes place when the spin-orbit interaction is weak compared to the electrostatic, the second when the electrostatic interaction is weaker. A third (jl) coupling takes place when the electrostatic interaction is weak compared to the spin-orbit interaction of the parent ion, but is strong compared to the spin coupling of the external electron.

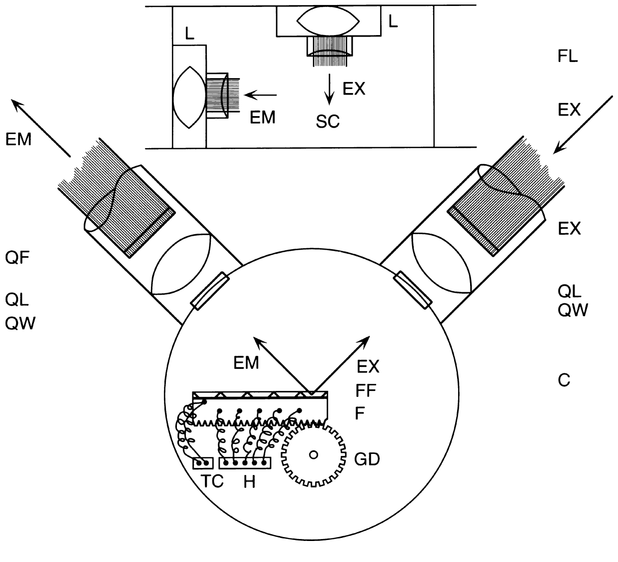

Figure 1. Low-temperature cryostat design to obtain optical emission spectra of silver chloroiodide emulsions. FL, spectrofluorimeter; L, lens assembly; EX, excitation optics; EM, emission optics; SC, sample chamber; QF, quartz fiber bundle; QL, quartz lens; QW, quartz window; C, cryostat; FF, film frame holder; F, cold block; H, heater; TC, thermal diode detector; GD, gear drive.

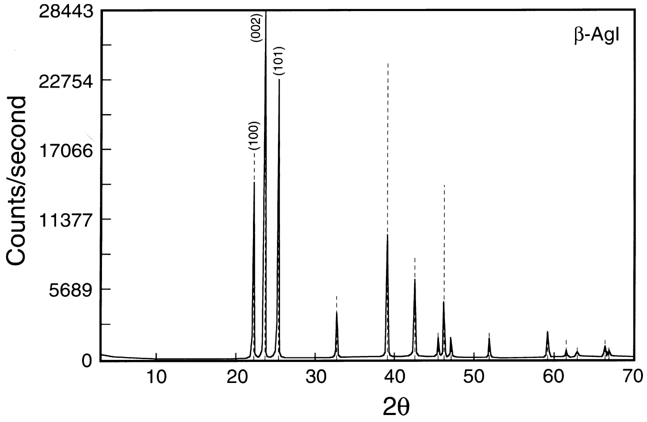

Figure 2. X-ray diffraction pattern of pure βAgI (wurtzite) hexagonal bipyramidal crystals in gelatin.

It was shown that the absorption cannot be thought of as a characteristic of the mixed crystal rather than as the sum of the individual components; e.g., the incorporated iodide anions produce well-defined absorption and emission bands resolved from the host absorption.[6a] Cardona[9] studied the absorption of thin films of AgI in the wurtzite and zinc-blend phases defining bands at 3.0 eV, 413 nm and 3.8 eV, 326 nm described as direct exciton absorption associated with the Γ_8 and Γ_6 valence bands, respectively. This is the spin-doublet that occurs when the iodide is either a $j = 3/2$ or $j = 1/2$ state. It was concluded that the discrete state formed by I^- in AgCl is related to the first exciton formation in AgI and can be described as a trapped exciton of the Wannier type, a state consistent with the low oscillator strength and small Stokes shift for emission discussed by Fowler and Dexter.[10]

Kanzaki, et al.[4,5] compared AgCl and AgCl,I 2.8×10^{-4} and 9.9×10^{-4} mole iodide/Ag mole at 4.2 K. The delayed emission contained two bands with peaks at 2.50 eV, 495.8 nm and 2.40 eV, 516.5 nm. The former is attributed to excitons bound at isolated iodide sites and the latter to those bound at iodide pairs. The relative intensity of the band at 2.40 eV, 516.5 nm increases in the delayed luminescence. These two bands have different decay kinetics, and this results in the shift of the emission spectra. The prompt luminescence of AgCl,I also contains two emission bands: a broadband at 2.43 eV, 510.1 nm, and another at 2.63 eV, 471.3 nm. In pure AgCl, only the 2.43 eV, 510.1 nm is observed and is assigned to excitons containing a self-trapped hole and an electron. The 2.63 eV, 471.3 nm is due to excitons bound at an iodide site.[6a]

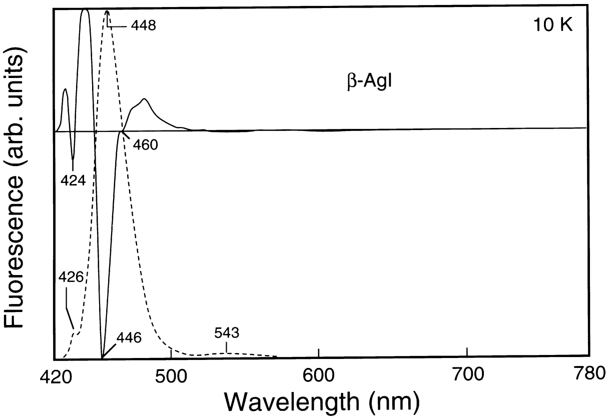

Figure 3. The 10 K photoluminescence, βAgI in gelatin, dashed line 426 and 448 nm maxima; second derivative, solid line 446 nm (Note: 424 and 446 nm band), excitation at 390 nm.

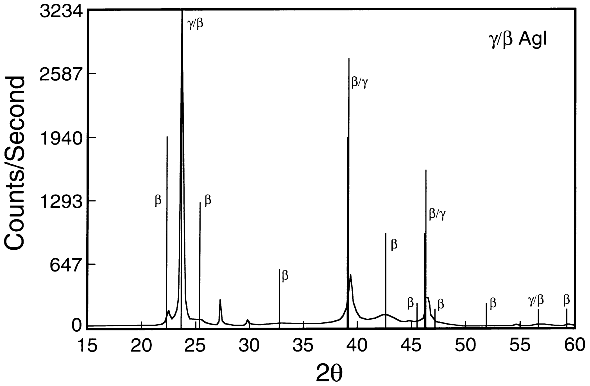

Figure 4. X-ray diffraction pattern of γAgI (sphalerite) cubic crystals in gelatin. A mixture of γ/β is observed under rigorous conditions of preparation.

Kanzaki and Sakuragi[11] also noted an extra absorption of AgCl,I; one is the low-energy band with Gaussian shape 3.13 eV, 396.0 nm, and the other is the component with multiphonon structures near the AgCl absorption edge ~3.25 eV, 381.4 nm. The intrinsic emission band of AgCl can be understood as the relaxation of the self-trapped hole (Ag^{2+} center) and an electron. This conclusion was supported by the transient optical absorption band at 1.2 eV, 1033 nm due to the self-trapped hole in AgCl under UV excitation at low temperatures.

Experimental

The instrumentation, that has been described previously, is shown[12–14] in Fig. 1. Films were coated with gelatin microcrystallite dispersions of nonsensitized silver chloroiodide cubes prepared at a vAg of 117 mV and a pH of 5.6. The coverage composition of the films were 350 mg gel/ft^2 and 300 mg Ag/ft^2. The film samples were

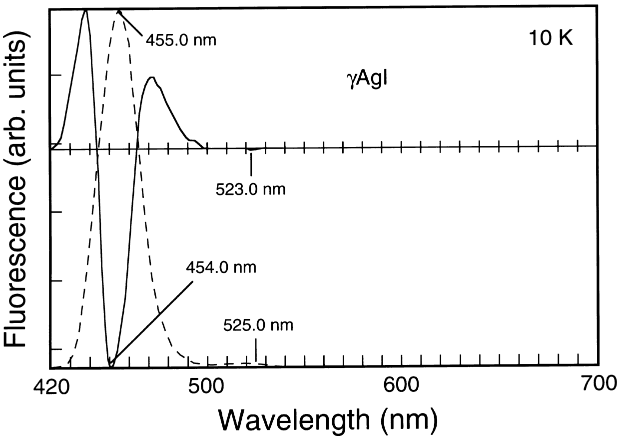

Figure 5. The 10 K photoluminescence, γAgI in gelatin, dashed line with a maximum at 455 and a minor at a 525 nm band; second derivative, solid line 454 nm maximum with a minor at a 523 nm band, excitation at 390 nm. The minor bands are assigned to Ag_n^0 clusters.

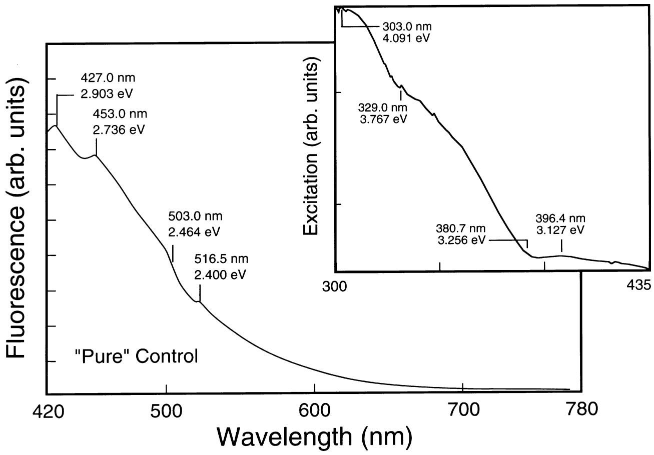

Figure 6. The 10 K photoluminescence of pure AgCl, 0.53 μm cubic dispersion. The excitation wavelength is 390 nm and the monitoring wavelength is 503 nm. Iodide impurity bands at 453.0 (γAgI) and 427.0 nm (βAgI) are noted in the emission spectrum. The free exciton iodide impurity absorption is seen at 303.0 nm, 4.091 eV; the indirect band gap at 380.7 nm, 3.256 eV; and a γAgI absorption at 396.4 nm, 3.127 eV.

held 20 min at the equilibrium temperature before spectroscopic analysis proceeded; new sample positions were irradiated for each temperature selected.

The control microcrystallites of βAgI were made from the double-jet KI and $AgNO_3$ precipitation; nucleated at 50°C for 0.5% of the make at 1.12 g/L KI, excess halide (–200 mV); and grown for the remaining part of the precipitation at 75°C. The final crystals were wurtzite, 0.67 μm hexagonal bipyramids. The γAgI sphalerite, cubic microcrystals 0.15 μm were prepared similarly with excess silver ion (+500 mV).

Results and Discussion

Optical Emission of AgI Microcrystallites. Figures 2 and 3 show the x-ray diffraction pattern of pure βAgI (wurtzite) hexagonal bipyramidal crystals in gelatin and the 10 K photoluminescence of the same sample, dashed line 426 and 448 nm maxima; second derivative, solid line 446 nm (note: 424 and 446 nm band) when excited at 390 nm. Figures 4 and 5 are the x-ray pattern of γAgI (sphalerite) cubic crystals in gelatin. A mix-

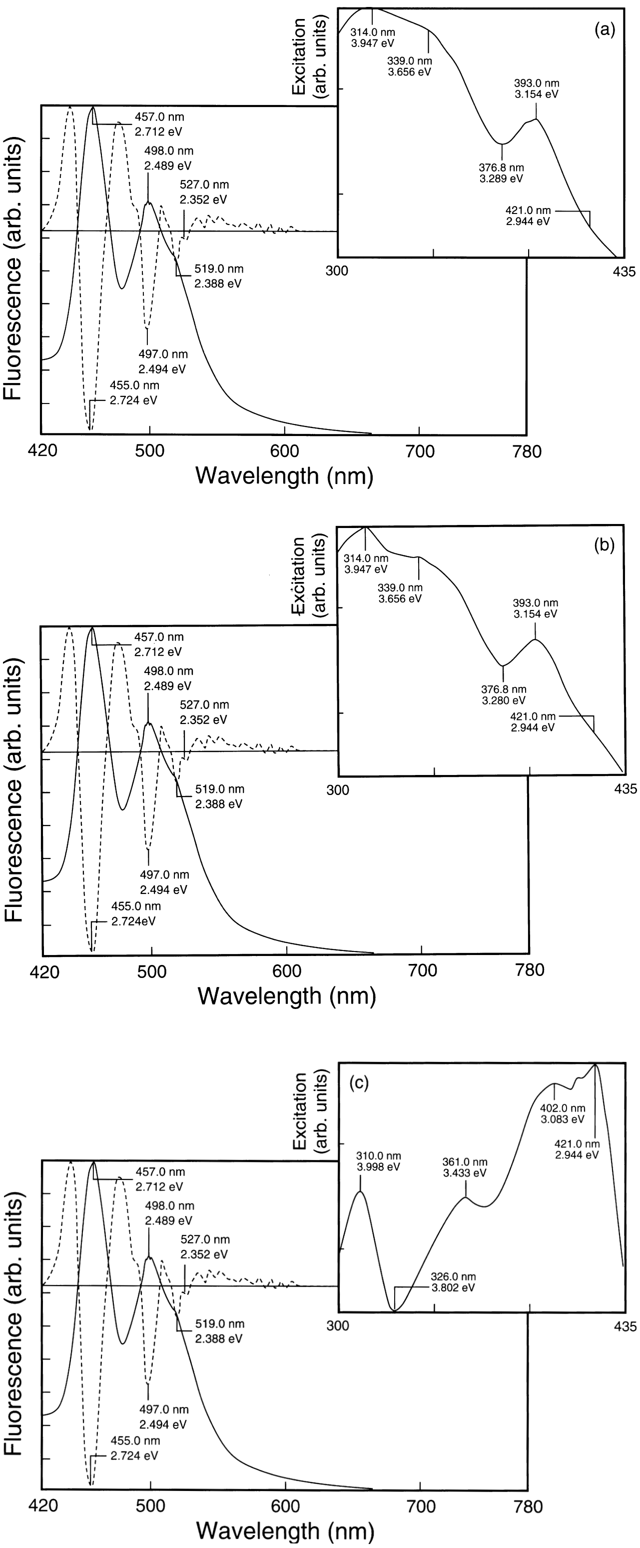

Figure 7. The 10 K photoluminescence of cubic, 0.57 μm edge, 99.5% AgCl, 0.5 M% KI was added at 93.8% of the growth cycle and held for 20 min without ripener. The excitation wavelength is 390 nm and the monitoring wavelengths are 519 (a), 497 (b), and 457 nm (c). The excitation (c) 421.0 is a γAgI absorption with 402 nm iodide absorption. The 361 and 310 nm are the free exciton bands for iodide impurity in AgCl. The dashed line is the second derivative of the emission spectrum with the excitation of 390 nm. Noteworthy is the 455 nm γAgI emission and the AgCl 497 nm excitons containing a self-trapped hole and an electron from bulk AgCl.

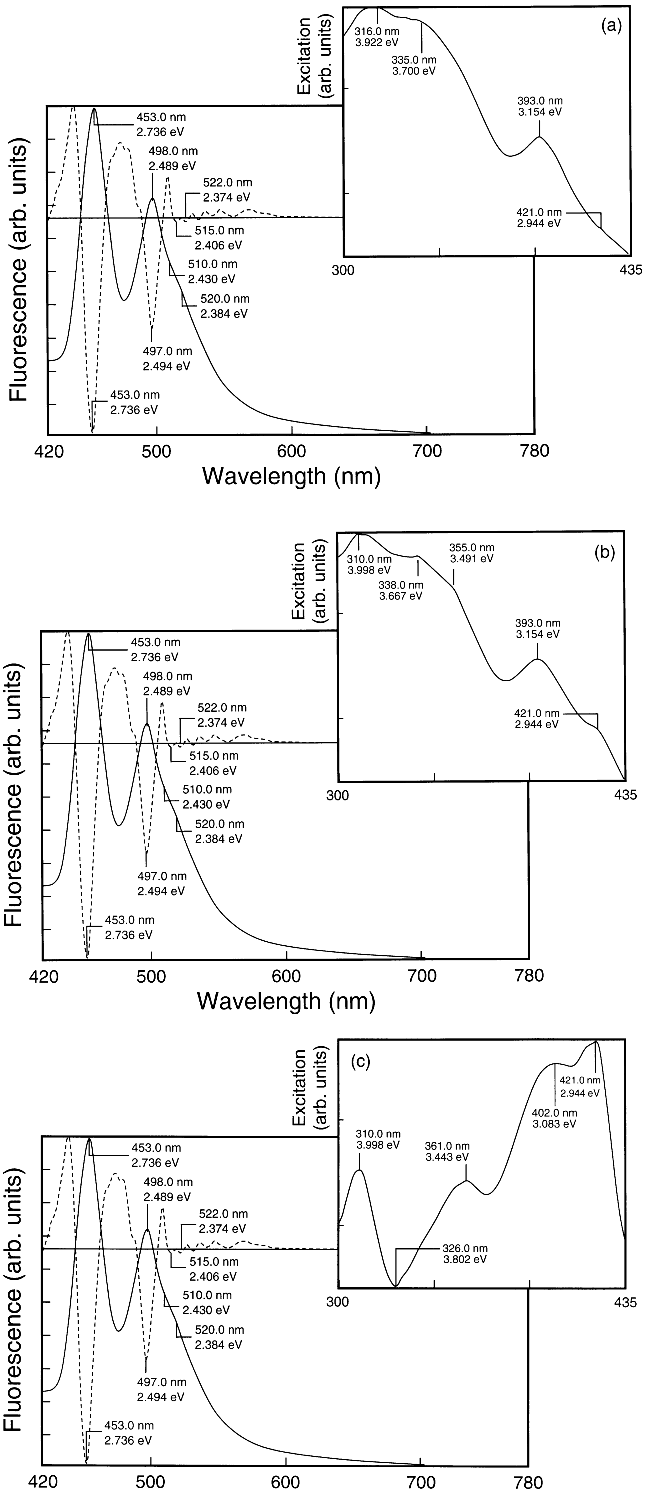

Figure 8. The 10 K photoluminescence of a tetradecahedral, 0.63 μm AgCl,I dispersion in gelatin, 99.5% AgCl, 0.5 M% KI was rapidly added at 93.8% of the growth cycle with no hold time, but ripener added. The excitation wavelength is 390.0 nm, 3.178 eV and the monitoring wavelengths are 515.0 nm, 2.406 eV (a), 497.0 nm, 2.494 eV (b), and 453.0 nm, 2.736 eV (c). The excitation (c) 421.0 nm, 2.944 eV is a γAgI cluster absorption with a 402.0 nm, 3.083 eV iodide absorption. The 361.0 nm, 3.433 eV and 310.0 nm, 3.998 eV are the free exciton bands of AgCl with an iodide impurity (excited states of $(\gamma AgI)_n$ clusters.) The dashed line is the second derivative of the emission spectrum with the excitation of 390.0 nm, 3.178 eV. The indirect AgCl band gap is seen (b) in the region of 380 nm, 3.26 eV.

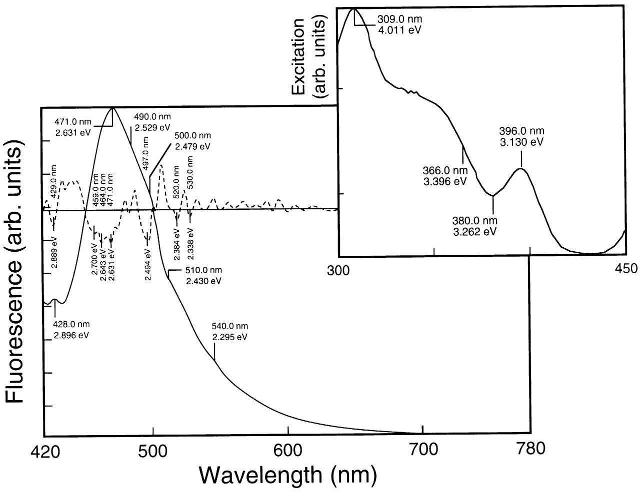

Figure 9. The 10 K photoluminescence of a cubic AgCl,I dispersion in gelatin, 0.75 μm edge length with composition of 99.8%, 0.27 M% KI added at 90.0% of the growth cycle over a 10-sec period with added ripener. The dashed line is the second derivative of the emission spectrum with excitation of 390.0 nm, 3.178 eV. The monitoring 471.0 nm, 2.631 eV, γAgI emission records the excitation or absorption spectrum relating to the 471.0 nm band (Figs. 7 and 8).

ture of γ/β is observed under rigorous conditions of precipitation. Again, the 10 K photoluminescence, γAgI in gelatin, is the dashed line with maxima at 455 and minor 525 nm which is assigned to Ag_n^0 clusters; second derivative, solid line 454 nm maxima with a minor 523 nm band is observed when excited at 390 nm. Figure 6 shows the 10 K photoluminescence of a pure AgCl, 0.53 μm-edge cubic dispersion in gelatin. This excitation spectrum 300–435 nm is monitored at 503 nm emission. The iodide absorption impurity band, the localized exciton of iodide, is noted at 396.4 nm, 3.127 eV, with the AgCl band edge at 3.256 eV, 380.7 nm. The two free exciton bands for AgCl with iodide impurity are seen near 3.767 eV, 329.0 nm and 4.091 eV, 303.0 nm. The emission curve when excited by 390 nm shows the impurity bands 2.903 eV, 427.0 and 2.736 eV, 453.0 nm with the AgCl localized exciton emission, the self-trapped hole (Ag^{2+}) with electron at 2.464 eV, 503.0 nm.

Figures 7(a) through 7(c) show the 10 K photoluminescence of a AgCl,I, 0.57 μm edge cubic dispersion in gelatin with a composition 99.5% AgCl, 0.5 M% KI added at 93.8% of the growth cycle and held for 20 min without ripener. The excitation wavelength is 390.0 nm, 3.178 eV and the monitoring wavelengths are 519.0 nm, 2.388 eV (a), 497.0 nm, 2.494 eV (b), and 457.0 nm, 2.712 eV (c). The excitation (c) 421.0 nm, 2.944 eV is a γAgI cluster absorption with a 402.0 nm, 3.083 eV iodide absorption. The 361.0 nm, 3.433 eV and 310.0 nm, 3.998 eV are the free exciton band of AgCl with an iodide impurity. The dashed line is the second derivative of the emission spectrum with the excitation of 390.0 μm, 3.178 eV. Noteworthy are the 455.0 nm, 2.724 eV γAgI cluster emission and the AgCl 497.0 nm, 2.494 eV excitons containing a self-trapped hole and a recombination emission from the excited electron.

Figures 8(a) through 8(c) show the 10 K photoluminescence of a AgCl, I, 0.63 μm edge tetradecahedral dispersion in gelatin with a composition of 99.5% AgCl, 0.5 M% KI rapidly added at 93.8% of the growth cycle

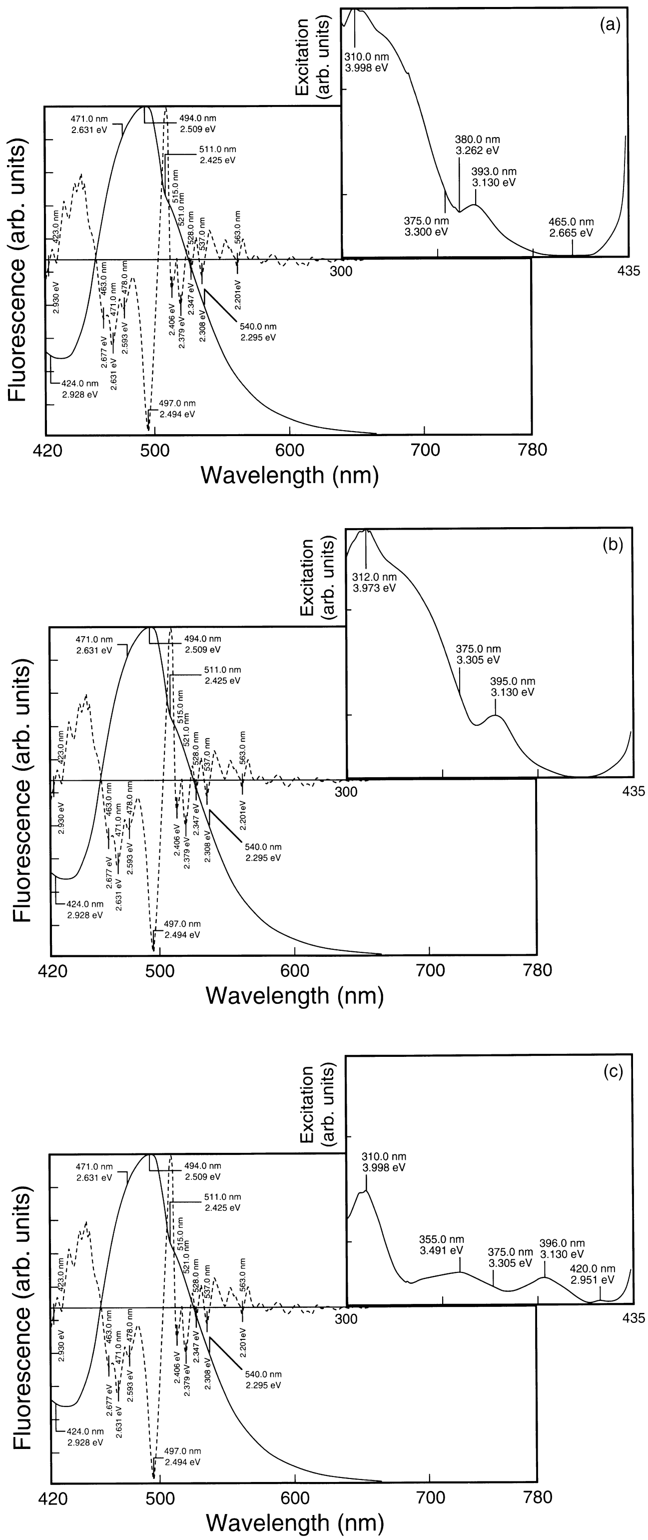

Figure 10. The 10 K photoluminescence of a AgCl,I, 0.75 μm edge cubic dispersion in gelatin with a composition of 99.8%, 0.2 M% KI added at 90% of the growth cycle over a 30-sec period with added ripener. The general overall features of the second derivative (dashed line) and the excitation spectra are similar to Figs. 7 through 9.

and no hold but added thioether ripener. The excitation wavelength is 390.0 nm, 3.178 eV and the monitoring wavelengths are 515.0 nm, 2.406 eV (a), 497.0 nm, 2.494 eV (b), and 453.0 nm, 2.736 eV (c). The excitation band (c) 421.0 nm, 2.944 eV is related to a γAgI cluster absorption with a 402.0 nm, 3.083 eV iodide absorption. The 361.0 nm, 3.433 eV and 310.0 nm, 3.998 eV are the free exciton bands of iodide in AgCl. The dashed line is the second derivative of the emission spectrum with the excitation of 390.0 nm, 3.178 eV. The indirect AgCl band gap is seen (b) in the 380 nm, 3.26 eV region. Noteworthy are the 453.0 nm, 2.736 eV, γAgI cluster emission and the AgCl 497.0 nm, 2.494 eV exciton containing a self-trapped hole and a recombination emission from the excited electron.

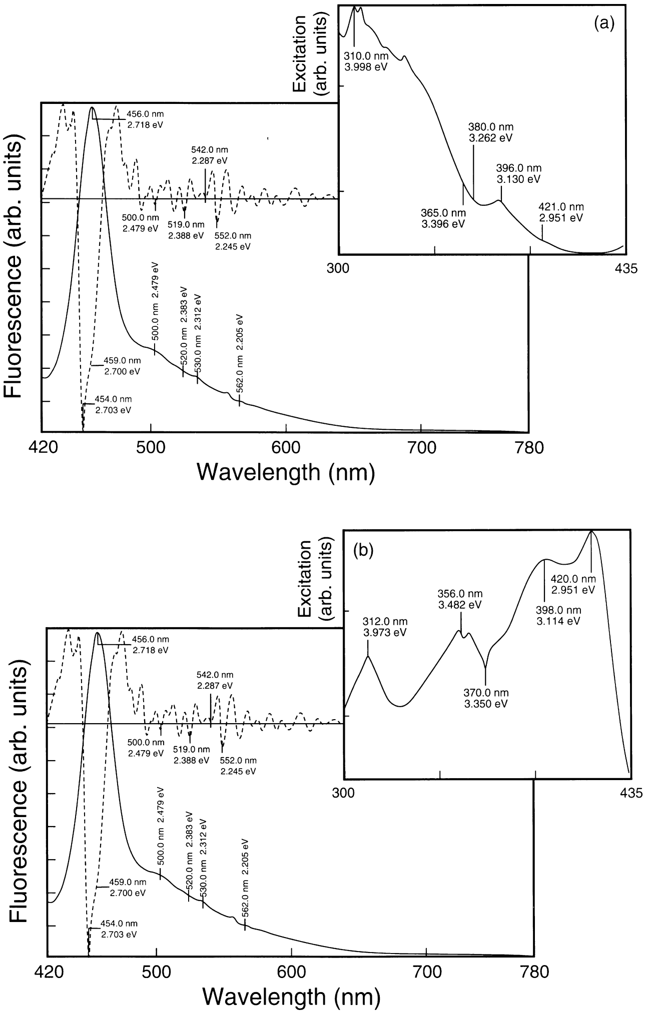

Figure 11. The 10 K photoluminescence of a AgCl,I, 0.74 μm edge length cubic dispersion in gelatin with a composition of 99.7%, 0.3 M% KI rapidly added at 93% of the growth cycle within a 1.0-sec interval with added ripener. The general overall features of the second derivative (dashed line) and the excitation spectra are similar to Figs. 7 through 10.

Figure 9 shows the 10 K photoluminescence of a AgCl, I, 0.75 μm edge cubic dispersion in gelatin with a composition of 99.8%, 0.2 M% KI added at 90.0% of the growth cycle with addition over a 10-sec period with added ripener. The excitation wavelength is 390.0 nm, 3.178 eV and the monitoring wavelengths are the same as previous examples of Figs. 7 and 8 with the shifted 453.0 nm to 471.0 nm, 2.632 eV. The monitoring wavelength of 471.0 nm is the emission of a larger γAgI cluster; the excitation spectrum shows the prominent

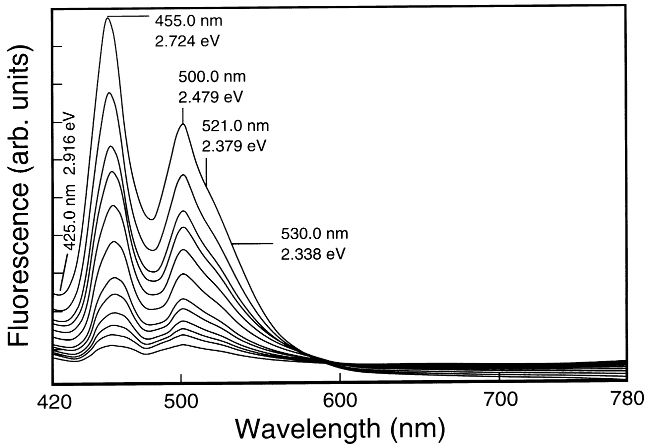

Figure 12. The 10 K photoluminescence of the tetradecahedral AgCl,I, 0.63 µm AgCl,I dispersion in gelatin, 99.5% AgCl, 0.5 M% KI rapidly added at 93.8% of the growth cycle with no hold time but ripener added. The fluorescence steady-state intensity versus wavelength is varied; i.e., neutral density filters were placed in the excitation light path.

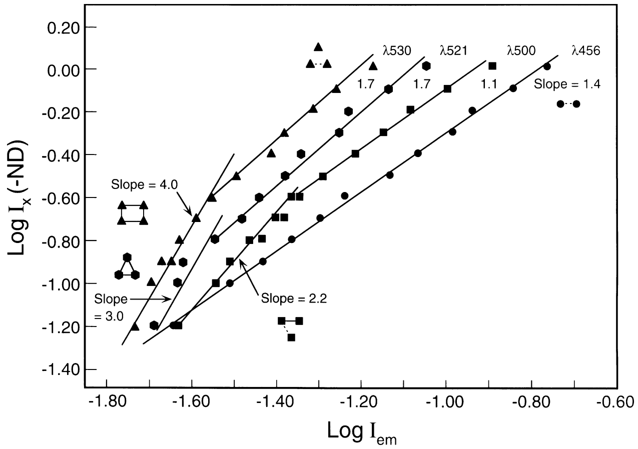

Figure 13. Plots of log I_x excitation versus log I_{em} emission yields changes in slope in the region of 500 to 530 nm with the exception of the γAgI cluster region of 456 nm. The slope *n* is related to the number of molecules or atoms within a cluster.

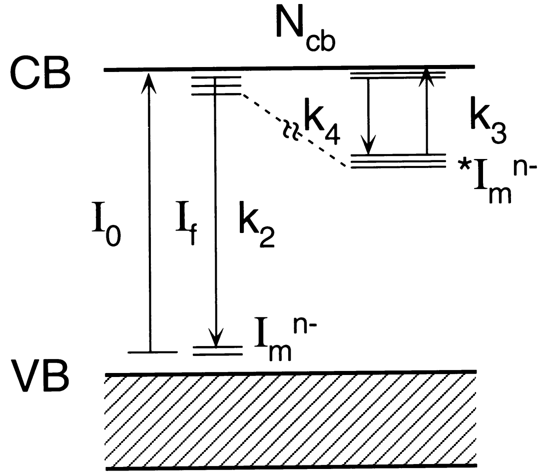

Figure 14. Simple energetic diagram of iodide recombination luminescence.

396.0 nm, 3.130 eV absorption for the γAgI clusters, the band gap transition in the range 360.0 nm, 3.396 eV and 380.0 nm, 3.262 eV, and the free exciton absorption of AgCl at 309.0 nm, 4.011 eV.

Figures 10(a) through 10(c) show the 10 K photoluminescence of a AgCl,I, 0.75 µm edge cubic dispersion in gelatin with a composition of 99.8%, 0.2 M% KI added at 90.0% of the growth cycle with addition over a 30-sec period with added ripener. The excitation wavelength is 390.0 nm, 3.178 eV and the monitoring wavelengths are 512.0 nm, 2.421 eV (a), 495.0 nm, 2.504 eV (b), and 450.0 nm, 2.754 eV (c). The excitation wavelength (c) 421.0 nm, 2.944 is assigned to a γAgI cluster absorption and the 393.0 nm, 3.154 eV to the iodide absorption. The 361.0 nm, 3.433 eV and 310.0 nm, 3.998 eV are the free exciton bands of an iodide impurity in AgCl. The dashed line is the second derivative of the emission spectrum with the excitation of 390.0 nm, 3.178 eV. Noteworthy are the triad 463.0 nm, 2.677 eV; 471.0 nm, 2.631 eV; and 478.0 nm, 2.593 eV γAgI cluster emissions and the AgCl 497.0 nm, 2.494 eV exciton containing a self-trapped hole and a recombination emission from the exciton electron. In addition, the prominent iodide emission bands in the 450 nm region in other samples due to mixing in the hold period are diminished and shifted to longer wavelengths: 471.0 nm, 2.631 eV, i.e., larger γAgI clusters. The band gap may also be seen in the 375.0 nm, 3.305 eV region. The general overall features of the second derivative (dashed line) and the excitation spectra are similar to Figs. 7 through 9.

Figures 11(a) and 11(b) show the 10 K photoluminescence of AgCl, I, 0.74 µm edge cubic dispersion in gelatin with a composition of 99.7%, 0.3 M% KI rapidly added at 93% of the growth cycle within a 1.0-sec interval with added ripener. The excitation wavelength is 390.0 nm, 3.178 eV and the monitoring wavelengths are 500.0 nm, 2.472 eV (a) and 456.0 nm, 2.718 eV (b).

The excitation, monitored at (b) 420.0 nm, 2.951 eV, is a γAgI cluster absorption with a 398.0 nm, 3.114 eV iodide absorption. The indirect band gap is observed in the region of 356 to 370.0 nm, 3.482 to 3.350 eV and at 310.0 nm, 3.973 eV the free exciton band of AgCl. When the emission monitoring wavelength is 500.0 nm, 2.479 eV (a), the emission of the AgCl bound exciton, the 421.0 nm, 2.951 eV iodide absorption, the 396.0 nm, 3.130 eV γAgI cluster absorption, and the AgCl indirect band-gap region are noted. The slight absorption is clearly seen at 420.0 nm, 2.951 eV, the γAgI cluster formation.

The dashed line is the second derivative of the emission spectrum with the excitation of 390.0 nm, 3.178 eV. Noted are the prominent γAgI, AgCl exciton electron recombination to the bound hole, and I_m^{n-} clusters assigned to 454 to 459, 500, and 519 to 542 nm, respectively.

Intensity Dependence of Iodide Centers within AgCl. The 10 K photoluminescence peak intensity dependence, when excited with 390.0 nm, 3.178 eV of varying intensities and with a photoenergy, is sufficiently energetic to stimulate band-to-band transitions in γAgI clusters, the indirect placement of the electron from the localized polyexciton levels to the conduction band. The monitoring of the recombination emissions due to the relaxation of the iodide excitons' trapping levels are observed at 456, 500, 521, and 530 nm, respectively (Fig. 12). The luminescence peak intensity, I_{em}, however, showed a superlinear dependence on the peak excitation intensity, I_x, in the iodide cluster region 521 to 530 nm (1.7) and γAgI cluster 456 nm (1.4), but a linear

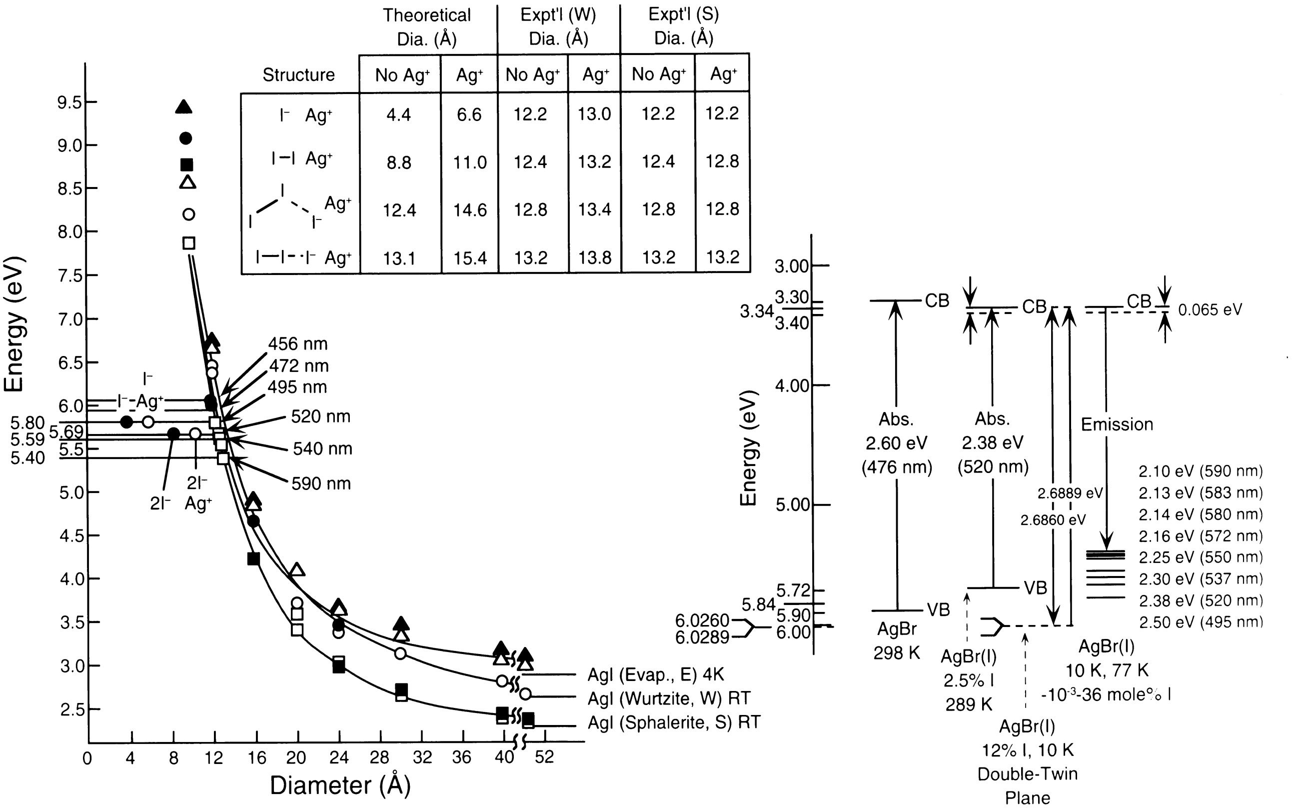

Structure	Theoretical Dia. (Å) No Ag^+	Theoretical Dia. (Å) Ag^+	Expt'l (W) Dia. (Å) No Ag^+	Expt'l (W) Dia. (Å) Ag^+	Expt'l (S) Dia. (Å) No Ag^+	Expt'l (S) Dia. (Å) Ag^+
I^- Ag^+	4.4	6.6	12.2	13.0	12.2	12.2
$I-I$ Ag^+	8.8	11.0	12.4	13.2	12.4	12.8
I I I^- Ag^+	12.4	14.6	12.8	13.4	12.8	12.8
$I-I\cdot\cdot I^-$ Ag^+	13.1	15.4	13.2	13.8	13.2	13.2

Figure 15. The correlation of the transition recombination energy at peak photoluminescence wavelength versus iodide cluster diameter. The Δ ○ □ and Δ ● ■ indicate band-gap values 2.93, 2.63, and 2.22 eV with estimated effective electron mass $m^*_{e^-}$ (0.286), (0.286) and effective hole mass $m^*_{h^+}$ (1.096), (0.60) paired, respectively, and the optical frequency dielectric $\in$ = 5.419 (500 nm).

dependence at 500 nm (1.1) or the direct recombination of the electron with localized hole on the iodide site, i.e., impurity dominated AgCl emission.

$$I_x = k\, I_m^{n-} \tag{1}$$

$$\log I_x = n \log I_{em} + \log k. \tag{2}$$

The slope n is related to the number of molecules or atoms within a cluster. A plot of log I_x excitation versus log I_{em} emission in Fig. 13 yields changes in slope in the region of 500 to 530 nm with the exception of the 456 nm γAgI cluster region. Note the greater slope changes for lower light intensity in the region 521 to 530 nm, 1.7, 1.7 (high intensity) to 3.0 and 4.0 (low intensity), respectively, reflecting structural changes. Due to the overlap of the AgCl emission band near 500 nm and the region of the iodide clusters, 572 to 530 nm, the slope for the I_m^{n-} would be expected to be more reliable (constant) furthest from the 500 nm wavelength, i.e., at 530 nm.

A kinetic derivation should give more insight to the luminescence processes. A simplified energetic diagram, Fig. 14, shows the rates or the probabilities of the transitions. The excited state of the luminescent center is shown very close to the conduction band. The $I_0 \alpha h \upsilon_x$ indicates the number of excitation events of the luminescent ground state centers per second and is proportional to the intensity of exciting light, absorbance by the luminescence center.

The quantities k_2 and k_4 are proportional to the effective cross sections of recombination and capture by a trap, respectively, and k_3 depends on temperature accordingly: $k_3 = k_3^0 \exp(-\Delta E/kT)$. The excitation rate for the number of excited iodide cluster centers is expressed as

$$-\frac{dI_m^n}{dt} = +I_0 I_m^{n-} - k_2(^*I_{m+}^{n-} + N_{cb}), \tag{3}$$

where N_{cb} is the number of electrons in the conduction band, I_m^{n-} is the ground state number iodide cluster sites. The number of iodide traps is greater than the number of captured electrons (absence of saturation) and is shown by

$$\frac{d{}^*I_{mx}^{n-}}{dt} = k_4 N_{cb} - k_3 {}^*I_{mx}^{n-}, \tag{4}$$

where $^*I_{mx}^{n-}$ is the number of electrons on the trap. The relationship of the number of ground state centers to the number of localized holes on the iodide sites (number of electrons on traps) and free electrons in the conduction band I_m^{n-}, $^*I_{mx}^{n-}$, N_{cb}, is, respectively,

$$I_m^{n-} = {}^*I_{mx}^{n-} + N_{cb}. \tag{5}$$

The number of electrons in the conduction band is seen to be $N_{cb} << I_m^{n-}$, $^*I_{mx}^{n-}$. We have assumed $^*I_{mx}^{n-} \approx I_m^{n-}$ (similar but not equal) and simplified by excluding N_{cb} from Eqs. 3 and 4. If light quanta of ν were emitted during the recombination at the I_m^{n-} site, then the intensity $I(t)$ at time t would be

$$I(t)\,\frac{h\nu dI_m^{n-}}{dt} = \frac{h\nu\left\{I_0 I_m^{n-} k_4 - k_2 k_3\left(I_m^{n-}\right)^m\right\}}{k_4 + k_2 I_m^{n-}} \quad \text{where } m \geq 2. \tag{6}$$

Two cases may be considered: (a) The probability of localization on a trap is smaller than the probability of the recombination with the localized trapped hole upon the I_m^{n-} site; i.e.,

$$k_4 N_{cb} << k_2 * \mathrm{I}_m^{n-} N_{cb}. \tag{7}$$

During the recombination or relaxation $\left(\mathrm{I}_0 \mathrm{I}_m^{n-} = 0\right)$, therefore,

$$\frac{d\mathrm{I}_m^n}{dt} = -k_3 * \mathrm{I}_{mx}^{n-}. \tag{8}$$

The analysis shows that the excited iodide centers decrease exponentially if $m = 2$ with the decay time determined by the probability of release from the traps beneath the conduction band. (b) However, due to the decreased excitation intensity, I_m^{n-} is excited to a lesser degree and the opposite inequality should be valid

$$k_4 N_{cb} >> k_2 * \mathrm{I}_m^{n-} N_{cb}. \tag{9}$$

Therefore

$$\frac{d\mathrm{I}_m^{n-}}{dt} = K - \frac{k_2 k_3 (*\mathrm{I}_m^{n-})^m}{k_4} \quad \text{where } m \geq 2 \tag{10}$$

and

$$K = \mathrm{I}_0 \mathrm{I}_m^{n-} / k_4 \tag{11}$$

As indicated in Eq. 6, the quadratic result is a function of the energy levels of the iodide structures and initial concentration of I_m^{n-} centers, i.e., the excitation intensity.

It is noteworthy to observe the higher slopes at longer wavelengths from the AgCl emission. These long-wavelength, higher slope species are attributed to iodide cluster size; e.g., 500 nm, 2.2 dimer; 521 nm, 3.0 trimer; and 530 nm, 4.0 and two dimers of iodide clusters. One alternate view may be in terms of the biexciton, triexciton, and di-biexcitons, again viewed in the 10 K photoluminescence (Fig. 13).

All of the structures can also be regarded as assemblages of I^- and/or I_3^- ions with I_2 molecules; $2\mathrm{I}^- + \mathrm{I}_2$, I_3^- or polyhalide anions of $\mathrm{I}_2\mathrm{Cl}^-$ or $\mathrm{I}Cl_2^-$ with Ag^+ cations.

Photoluminescence and the Relationship to Iodide Cluster Diameter. Figure 15 shows the energy of the lowest excited electronic state (i.e., the conduction band plus the transition recombination energy at the peak photoluminescence wavelength) versus the small iodide cluster diameter.

These curves, derived from Eq. 12, are used to determine the iodide cluster size.[15–22]

The theory relates the size of small clusters to quantized energy levels, the spacing between the adjacent states being of the order E_f/N, where E_f is the Fermi energy and N is the number of atoms in a cluster. Because E_f has a value of a few electron volts, the energy levels in a cluster of 10^{+3} to 10^{+1} atoms are separated by about 10^{-3} to 10^{-1} eV, as seen in Fig. 15 for photoluminescence of iodide centers. The particle-in-a-box theory is applied and was presented previously[12,13,23] but with inclusion of the Ag^+ within the AgBr matrix. Allowance has been made in Fig. 15 for the Ag^+–I^- bonding. The optical frequency dielectric[16,24] for AgI (486 nm) $\in = 5.419$ is inserted in the Coulomb attraction term and the third-solvation energy-loss term is not applicable.[12,13,23] The effective masses $m_{e^-}^*, m_{\hbar^+}^*$ of electrons and holes are approximated from literature values by comparing semiconductor properties.[25,26] Silver bromide effective masses have been used as a reference. In terms of an overlap model,

$$\mathrm{Eg(R)} = \mathrm{Eg(R} = \infty) + \frac{\hbar^2\pi^2}{2R^2}\left[\frac{1}{m_{e^-}^*} + \frac{1}{m_{\hbar^+}^*}\right] - \frac{1.8e^2}{\in R} + \frac{e^2}{R}\sum_{n-1}^{\infty}\alpha_n\left(\frac{S}{R}\right)^{2n}, \tag{12}$$

the larger the overlap of wavefunctions of the holes and electrons between different atoms or ions, the wider the band state becomes; the wider this band, the smaller the effective mass. The effective electrons $m_{e^-}^*$ (0.286), (0.286) and the effective holes $m_{\hbar^+}^*$ (1.096), (0.60) paired, respectively, for two trial calculations, are shown in the second confinement energy term for the allotropic forms of AgI. The $Eg(R = \infty)$ is taken as a reference energy at room temperature of the βAgI wurtzite band gap (2.63 eV) and of the (2.22 eV) band gap of sphalerite, γAgI. The $Eg(R)$ is the recombination emission to states representing the quantum size (R) radius of the iodide aggregates. An evaporated film of 2.92 eV band gap at 4 K is also considered with each of the paired effective masses for holes and electrons.

AgBr,I. The quantum cluster iodide emission spectra are quite different from those for bulk AgI material. The different configuration and complex structures of iodide within the AgBr lattice can be related to the low-temperature photoluminescence spectra.[14] The 540-nm region represents a suggested bent I_3^- anion, or $(\mathrm{AgI}_3)_n$ assuming a theoretical diameter of (12.4 Å without Ag^+) 14.6 Å as the long axis of the triangle versus 13.4 Å for wurtzite (W) and 12.8 Å for sphalerite (S) calculated diameters (including Ag^+ bond) observed[14] from the emission-spectroscopic-curve analysis (Fig. 15). The calculated confinement volume of the exciton is 1259 Å^3 (W) and 1098 Å^3 (S) for the bent iodide. Cubic sphalerite 4 molecules/unit lattice has a unit cell volume of 273.89 Å^3, that yields[14] 64 atom/cluster or 16 molecule/cluster $(2\mathrm{I} - \mathrm{IAg}^+)_n$. The wurtzite hexagonal 2 molecule/unit lattice structure has a unit cell volume of 137.2 Å^3, that yields[14] 72 atom/cluster or 18 molecule/cluster.[14]

The 590 nm region emission was not present but was observed in previous studies[1a,b] related to a linear structure of 13.8 Å (W) diam versus 13.2 Å (S) for wurtzite and sphalerite allotropic forms, respectively. Again, the calculated confinement volume of the exciton is 1376.1 Å^3 (W) and 1204.3 Å^3 (S) for the 4 atom (3 iodide 1 silver) linear molecules and yields 20 molecule/cluster or 80 atom/cluster for hexagonal wurtzite structures. The cubic sphalerite form approximates 18 molecule/cluster or 72 atom/cluster for the linear-arranged clusters. Longer wavelength bands, overlapping the 562 to 571 nm unstable Ag_3^0 emissions,[1a,b] are interpreted as larger clusters of I_m^{n-} in the presence of Ag^+. These structures are emitting radiation not as AgI, but as larger domains of iodide near silver centers in the AgBr lattice. A deviation is seen (Fig. 15) for the 520 nm two-atom iodide molecule exciton,[9,13] the diameter of which should be 8.76 Å, I–I or 11.0 Å I–I-Ag^+ versus the experimentally (spectroscopic energy versus diameter graph) calculated diameter of 13.2 Å. A deviation is also seen for the 1-atom-diam iodide center, calculated 4.4 Å, I^- or $\mathrm{I}^-\mathrm{Ag}^+$ 6.6 Å (Eq. 12).[27,28] A summary of the data is shown in Table I. Can quantum clusters of such small magnitudes possess cubic or hexagonal symmetry? Note in Fig. 15 the curves (symmetry) converge at small radii.[14]

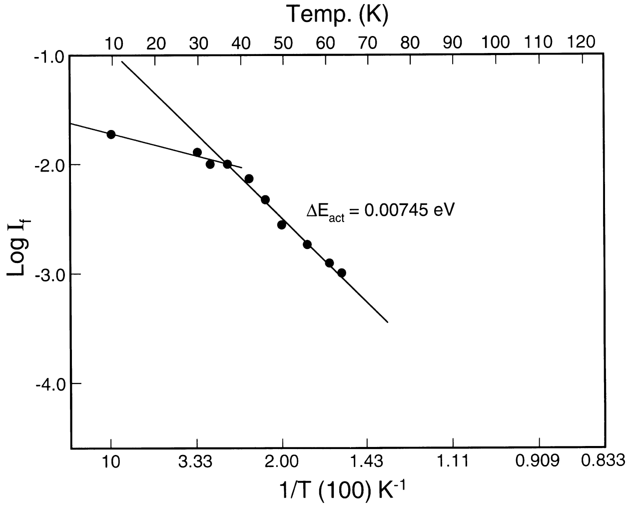

Figure 16. The steady-state peak photoluminescence, sample from Figs. 8 and 12, $\log I_f$ (γAgI) at 456 nm, 2.718 eV versus the reciprocal temperature. The $\Delta E_{act} = 0.00745$ eV with the extrapolated intercept -0.62 = ln K_0; $\Delta S^{\ddagger} = -0.00244$ eV/deg mole. (The AgCl 99.5 M%, 0.5 M% KI was added rapidly at 93.8%, no temperature hold but added ripener.)

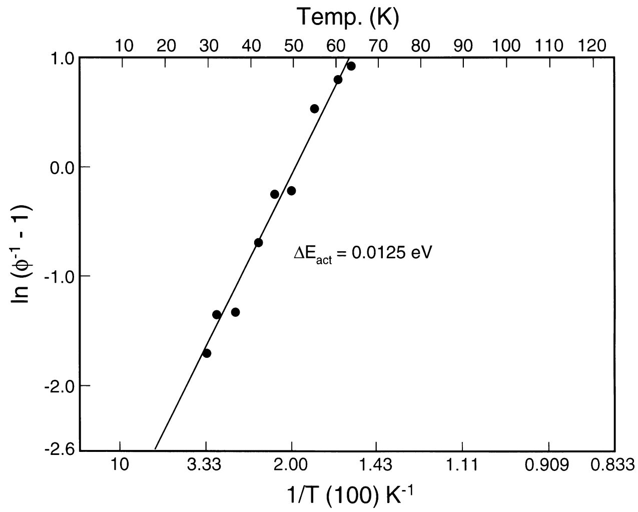

Figure 17. A plot of the photoluminescence quantum efficiency, $\ln(\phi^{-1} - 1)$ versus the reciprocal temperatures, $1/T$, for the 456.0 nm, 2.718 eV, γAgI cluster; $\Delta E_{act} = 0.0125$ eV. (The AgCl 99.5 M%, 0.5 M% KI was rapidly added at 93.8% growth, no temperature hold but added ripener.)

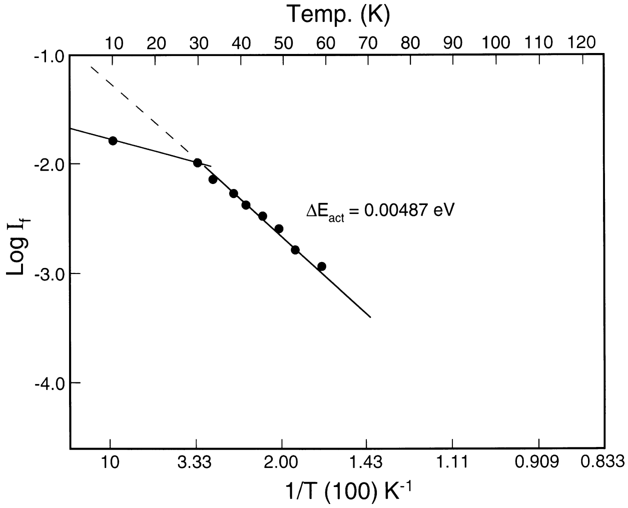

Figure 18. The temperature dependence of the peak photoluminescence, $\log I_f$(γAgI) at 456 nm, 2.718 eV versus the reciprocal temperature. The $\Delta E_{act} = 0.00487$ eV with the extrapolated intercept -0.96 = lnK_0; $\Delta S^{\ddagger} = -0.00248$ eV/deg mole. (The AgCl 99.5 M%, 0.5 M% KI was added rapidly at 96.0% with no temperature but added ripener.)

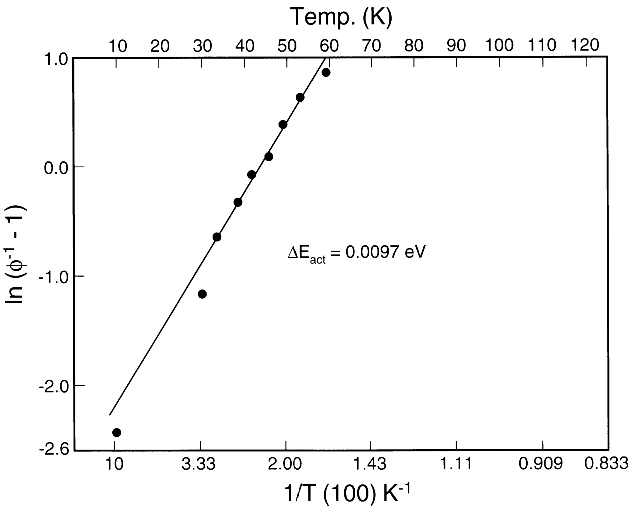

Figure 19. A plot of the photoluminescence quantum efficiency, $\ln(\phi^{-1} - 1)$ versus the reciprocal temperature, $1/T$, for the 456.0 nm, 2.718 eV, γAgI cluster; $\Delta E_{act} = 0.0097$ eV. (The AgCl 99.5 M%, 0.5 M% KI was rapidly added at 96.0% growth with no temperature hold but added ripener.)

The HOMO, hole-trapping species of the iodide center has been observed by the photoluminescence; the LUMO, lowest unoccupied molecular orbital, for the iodide electron-trapping AgBr,I tabular nonstriation grain center is 0.065 eV beneath the conduction band whereas the striation electron-trapping center is 0.055 eV beneath the conduction band.[14] It is concluded[14] that the emission assignments take into consideration these shallow electron traps at room temperature (Fig. 15).

AgCl,I. The 456.0 nm, 2.718 eV region represents a gAgI cluster with a diameter of 12.3 Å. However, a long-wavelength shift is observed to 471.0 nm, 2.631 eV as a function of addition rate and hold time for iodide. At longer addition times, the diameter increased to 12.7 Å, (Eq. 12 and Fig. 15). The wavelength of 456 nm indicates a sphalerite cubic γAgI crystallite formation with a lattice constant of 6.495 Å having a cubic cell volume of 273.99 Å^3 unit cell; therefore, 3.556 unit cells are formed each with 4 molecule/unit cell. Thus 14.22 γAgI molecules have been detected in a sphere with a 12.3 Å diam or exciton volume of 974.35 Å^3. Another way to calculate the number of γAgI molecules in a cubic configuration would be to assume the 12.3 Å diam to be the edge length, yielding an exciton volume of 1,860.87 Å^3/273.99 Å^3/unit cell = 6.791 unit cells or 27.17 γAgI molecules.

When the cluster diameter increased from 12.30 Å to 12.69 Å, the number of γAgI molecules per cluster increased from 14.22 to 15.62 and 27.17 to 29.83 when a spherical or cubic model had been calculated, respectively, as shown in the previous calculations.

Temperature Dependence. Figure 16 (Figs. 8 and 12 are similar samples) shows the steady-state peak photoluminescence (signal voltage) in vacuum of AgCl, I, 0.63 μm edge tetradecahedral dispersion in gelatin with a composition of 99.5% AgCl, 0.5 M% KI rapidly added at 93.8% of the growth cycle with no temperature hold but added ripener. The excitation wavelength is 390.0 nm, 3.178 eV and emission monitored in the range of 420 to 800 nm. The log photoluminescence 456.0 nm, 2.718 eV versus the reciprocal temperature, an Arrhen-ius plot, shows a change in slope near 37 K. The steeper slope, ΔE_{act} = 0.00745 eV, is indicative of a very shallow electron trap beneath the conduction band. The extrapolated intercept is -0.62; $\Delta S^{\ddagger} = -0.00244$ eV/deg mole. Figure 17, the plot of photoluminescent quantum efficiency $\ln(\varphi^{-1} - 1)$ versus 1/T, should yield a straight line the slope of that gives $-(\Delta E_{act}/k)$, and the intercept n with the $\ln(\varphi^{-1} - 1)$ axis yields $\ln K_0$ as derived in Eqs. 13 and 14.

$$\phi = \frac{R}{R+NR} = \frac{1}{1+\frac{NR}{R}} = \frac{1}{\left[1+K_0 \exp\left(\frac{-\Delta E_{act}}{kT}\right)\right]}. \qquad (13)$$

The (NR/R) contains the Boltzmann factor $A \exp[(\Delta E_{act}/kT)]$, where A is the vibrational frequency (60 K:$1.23 \times 10^{+12}$ $\sec^{-1}$) of the system in the excited state and the entropy contribution is considered negligible, k is the Boltzmann constant, and T is the absolute temperature. A transfer coefficient is introduced with values of 0 to 1, in order to account for the electron probability of returning to the conduction band and subsequently k_2 to the recombination center. The value K_0 is defined as tA/R without the entropy terms $e(\Delta S_{act}{}^{+}/k)$ for NR and R components. A transformation of Eq. 13 leads to

$$\ln\left(\phi^{-1} - 1\right) = \ln K_0 - \frac{\Delta E_{act}}{kT}. \qquad (14)$$

The ΔE_{act} energy reflects the shallow electron trap energy beneath the conduction band as 0.0125 eV. The fundamental data of Fig. 17 yield a plot of the quantum efficiency against reciprocal temperature. The initial invariant part of the curve represents $\phi = 1$. All the curves reference the highest signal as $\phi = 1$. It was assumed that ΔE_{act} was independent of temperature. Because the lattice vibrations are a function of temperature and the equilibrium configuration of the ions and the substitutional dopants such as iodide ions are also a function of temperature, ΔE_{act} should also be expressed accordingly as a function of temperature and should take the form of a polynomial expansion similar to the heat capacity, i.e., $\Delta E = \Delta E_0 + \alpha T + \beta T^2$ where ΔE_0 is the ΔE at absolute zero. In addition, the ratio of the NR/R term is related in a more complex relationship than presented in Eq. 13, the pre-exponential term should also include the entropy terms. The assumption of the transmission coefficient being equal to 1 is a simplification, likewise the omission of the tunneling factor.

Figures 18 and 19 are plots of the temperature dependence for γAgI clusters assigned to the 456.0 nm, 2.718 eV emission. The dispersion is a 0.77 nm AgCl, I cubic dispersion in gelatin with a composition of 99.5% AgCl, 0.5 M% KI rapidly added at 96.0% of the growth cycle with no temperature hold but added ripener. The Arrhenius plot for the ΔE_{act} yields 0.00487 eV and the extrapolated intercept for $\ln A$ (the pre-exponential term) is –0.96 (Fig. 17); $\Delta S^{\ddagger} = -0.00248$ eV/deg mole. Figure 19 yields an ΔE_{act} of 0.0097 eV, for the plot of $\ln(\phi^{-1}-1)$ versus $1/T$.

Figure 20(a) is the 10K photoluminescence spectrum of the AgCl,I (0.5 M%) with a dopant incorporated, while Figs. 20(b) and 21 are plots of the temperature dependence for γAgI clusters assigned to 456.0 nm, 2.718 eV emission. The dispersion is a 0.71 μm AgCl,I cubic dispersion in gelatin with a composition of 99.5% AgCl, 0.5 M% KI rapidly added at 93.0% of the growth cycle with no temperature hold but added ripener and a dopant of $Cs_2[Os(NO)Cl_5]$, 5 μg/Ag mole. The Arrhenius

TABLE I. Recombination Photoluminescence from Doped Iodide Centers in Cubic Silver Chloride Dispersions

Literature	Temp (K)	Lum. peak (nm)	Suggested luminescence centers
Ehrlich	10	448, 456	βAgI off grain, γAgI incorporated clusters
		512–540	I_m^{n-}-mers incorporated
		560–570	Ag_n^0 clusters
Farnell et al.[2]	77	435.6–546.1 (dispersion)	AgCl,I localized hole on iodide site as recombination center
Czaja and Baldereschi[29]	10	469.3 (AgBr crystals)	AgBr,I, iodide hole trap with phonon interactions
Belous et al.[30]	77	530, 560	I_2^{2-} dimers
		421, 455–460 (dispersion)	γAgI clusters with AgCl, AgBr grains
		440–445 (dispersion)	βAgI clusters with AgCl, AgBr grains
Moser et al.[6a]	5–77	380 abs, 396 abs and 415 abs crystals, sheet crystals 464	AgCl, AgCl,I, bound exciton I_2^{2-} iodide bound hole and recombination center
Kanzaki and Sakuragi[11]	2	380 and 396 abs (crystals)	AgCl, AgCl,I
		466, 505 (crystals)	AgCl,I, AgCl electron bound around self-trapped hole at iodide site, intrinsic luminescence by electron and self-trapped hole

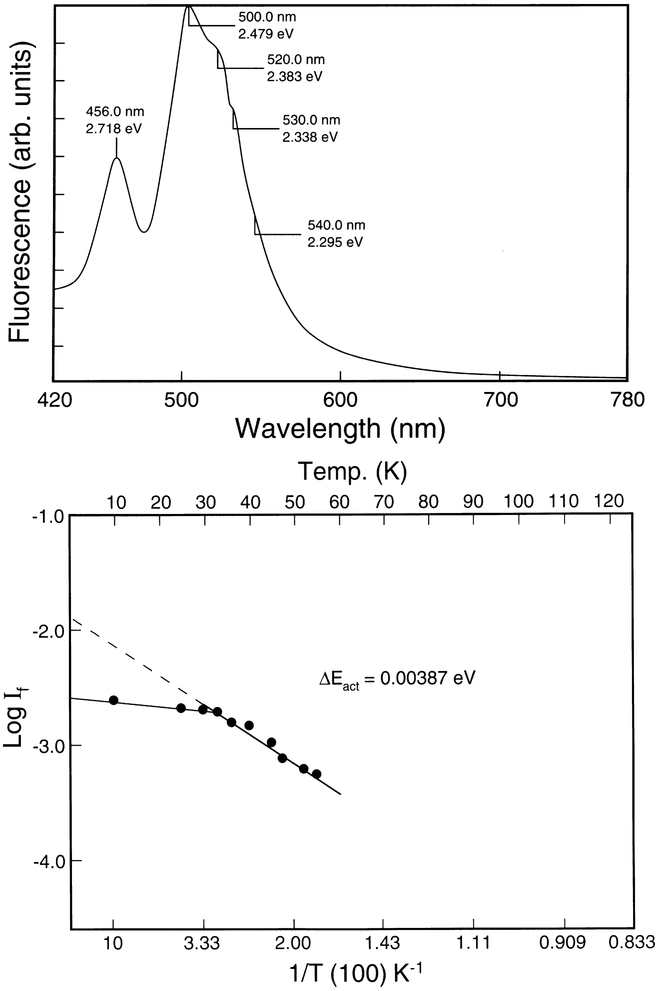

Figure 20. (a) The 10 K photoluminescence, 0.71 μm cubic AgCl 99.5 M%, KI 0.5 M% added at 93% growth with dopant $Cs_2[Os(NO)Cl_5]$ 5 μg/Ag mole. (b) The steady-state peak photoluminescence, logI_f (γAgI) at 456 nm, 2.718 eV versus the reciprocal temperature. The ΔE_{act} = 0.00387 eV with the extrapolated intercept -1.86 = lnK_0. The dopant of $Cs_2[Os(NO)Cl_5]$ 5 μg/Ag mole has been incorporated.

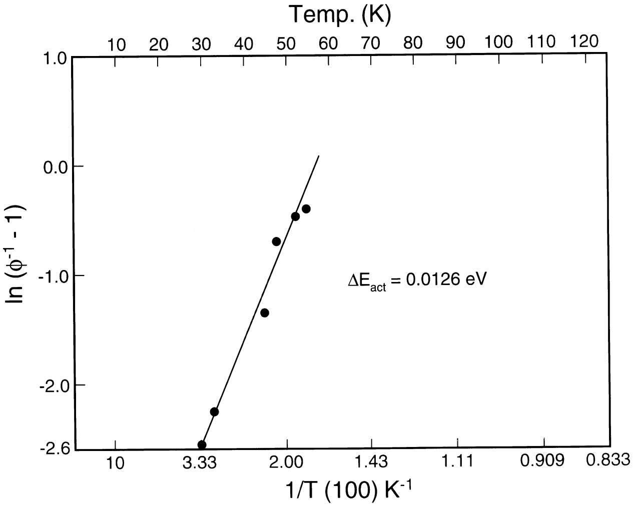

Figure 21. A plot of the photoluminescence quantum efficiency, ln(ϕ^{-1}–1) versus the reciprocal temperature, $1/T$, for the 456.0 nm, 2.718 eV γAgI cluster; ΔE_{act} = 0.0126 eV. The dopant of $Cs_2[Os(NO)Cl_5]$ 5 μg/Ag mole has been incorporated. The sample is the same as shown in Figs. 20(a) and 20(b).

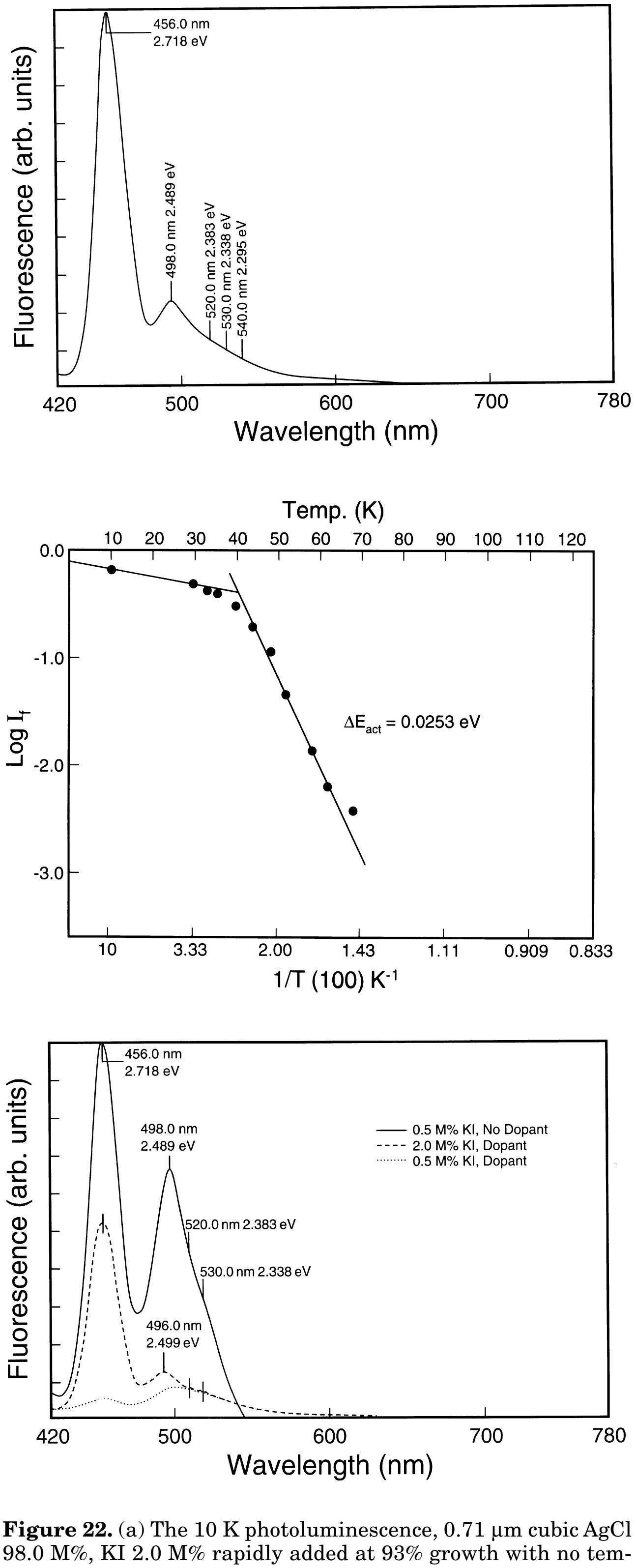

Figure 22. (a) The 10 K photoluminescence, 0.71 μm cubic AgCl 98.0 M%, KI 2.0 M% rapidly added at 93% growth with no temperature hold, but ripener added with a dopant $Cs_2[Os(NO)Cl_5]$ 5 μg/Ag mole. (b) The steady-state peak photoluminescence, logI_f (γAgI) at 456 nm, 2.718 eV versus the reciprocal temperature. The ΔE_{act} = 0.0253 eV with the extrapolated intercept +4.00 = ln K_0; $\Delta S^{\ddagger}$ = -0.00205 eV/deg mole. The dopant of $Cs_2[Os(NO)Cl_5]$ 5 μg/Ag mole has been incorporated. (c) A summary of three conditions involving electron competition shown in terms of the reduced γAgI (λ453 to 456 nm) emission: a control, 0.5 M% KI, without dopant; 0.5 M%; and 2.0 M% KI with 5 μg/Ag mole dopant. Note the emission quenching due to the presence of the dopant.

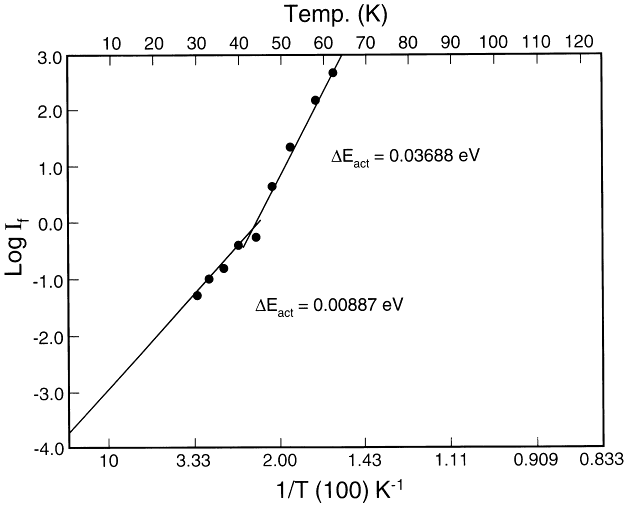

Figure 23. A plot of the photoluminescence quantum efficiency, $\ln(\phi^{-1} - 1)$ versus the reciprocal temperature, $1/T$, for the 456.0 nm, 2.718 eV, γAgI cluster; ΔE_{act} = 0.0368 eV. A second electron trap is observed via the second ΔE_{act} = 0.00887 eV with an extrapolated intercept –3.60 = $\ln K_0$.

plot for the ΔE_{act} yields 0.00387 eV and the extrapolated intercept of -1.86 for $\ln A$ (the pre-exponential term) Fig. 20; $\Delta S^{\ddagger}$ = -0.00256 eV/deg mole. Figure 21 shows the plot of the photoluminescence quantum efficiency versus reciprocal temperature and produced an ΔE_{act} of 0.0126 eV with the incorporated dopant mentioned above.

Figure 22(a) is the 10 K photoluminescence spectrum of the AgCl,I (2.0 M%) with a dopant incorporated while Figs. 22(b) and 23 are similar to 19 and 20a; however, the dispersion is a cubic 0.71 μm AgCl,I in gelatin with a composition of 98.0% AgCl, 2.0 M% KI rapidly added at 93% of the growth cycle with no temperature hold but added ripener and a dopant of $Cs_2[Os(NO)Cl_5]$ 5 μg/Ag mole. The Arrhenius curve of steeper slope yielded an ΔE_{act} of 0.0253 eV and an extrapolated intercept of +4.00 for $\ln K_0$ (the pre-exponential term); $\Delta S^{\ddagger}$ = –0.00205 eV/deg mole (Fig. 22). Figure 22(c) shows three conditions involving electron competition in terms of the γAgI reduced emission caused by the dopant.

A summary of the three conditions are the following: (1) A control without dopant, (2) 0.5 M% KI with dopant, and (3) 2.0 M% KI with dopant at the same position of incorporation.

The ratio of intensities λ 456/l 500 nm, i.e., γAgI/AgCl, is 4.27 for 2.0 M% KI, 0.63 for 0.5 M% KI, and a control without the dopant but with 0.5 M% KI is 1.405. Therefore, it may be inferred that the competitive trapping of the electron by the dopant, instead of recombination emission may be occurring. The dopant is reducing the photoluminescence by 44.9% when the iodide concentration is 0.5 M% and by 24.1% when KI is 2.0 M%.

Figure 23 shows the plot of the photoluminescence quantum efficiency versus the reciprocal temperature and produced a ΔE_{act} = 0.0368 eV. It is noteworthy to mention a break in the curve near 42.5 K with an ΔE_{act} = 0.00887 eV and an extrapolated intercept of -3.60 for $\ln A$ (the pre-exponential term) Fig. 23. The higher iodide concentration in the presence of the dopant $Cs_2[Os(NO)Cl_5]$ 5 μg/Ag mole has increased the depth of the electron trap or provided a new or deeper trap. The shallower trap is still observed. It may be stated that the (LUMO) of the iodide species is positioned very close to the conduction band and is a function of concentration and depth beneath the crystal surface. The negative $\Delta S^{\ddagger}$ term indicates a more rigid transition state (trap – electron complex) than the reactants (trap + electron). Table I is a summary of photoluminescent iodide centers doped in silver chloride dispersions.

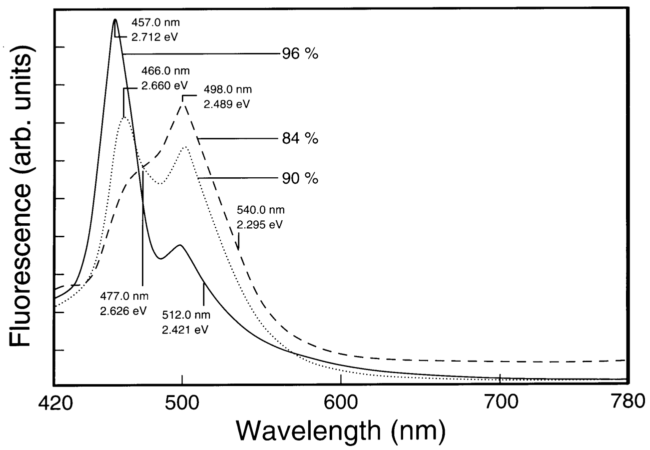

Figure 24. The rapid incorporation of 0.5 M% KI to 99.5 M% AgCl added at 84.0, 90.0, and 96.0% of the growth cycle. The final edge length is 0.77 μm cubic dispersion within gelatin, when ripener had been added. Note: The volume of the crystallite is 96.0% of the growth cycle when 0.5 M% KI is added; hence the I_m^{n-} is saturated in a 4.0% volume shell or 25 times the initial concentration. The saturation of 7.1 M/V% precipitates the γAgI phase. The emission from the assigned γAgI clusters diminish as the bound hole recombines with the electron of the AgCl exciton and the latter emission increases, proceeding from the 96% to 84% position in the growth cycle.

Subsurface Iodide Doping. Figure 24 shows the 10 K photoluminescence of dispersions with 0.77 μm edge cubic AgCl,I in gelatin with a composition of 99.5 M% AgCl, 0.5 M% KI rapidly added at 84, 90, and 96% of the growth cycle and no temperature hold but with added ripener. The 84% growth with iodide addition shows the largest wavelength shift to 477.0 nm, 2.626 eV from 90%, 466.0 nm, 2.660 eV with the reference at 96% or 457.0 nm, 2.712 eV. The rapid addition of KI closer to the surface increases the intensity and sharpens the γAgI cluster spectra which correlated with the photographic response. When the intensity of γAgI is prominent, the intrinsic photoluminescence from the AgCl crystals is reduced in the region of 498.0 nm, 2.489 eV as well as in the shoulder in the I_m^{n-} dimer region of 512.0 nm, 2.421 eV to 530.0 nm, 2.338 eV. The particle diameter of γAgI is 12.3 Å, a minimum at 96% when the iodide is introduced and increased in diameter to 12.7 Å at 84% growth of the cubic AgCl crystals (7.458 unit cells, 29.83 γAgI molecules). This issue has been discussed in the section Photoluminescence and the Relationship to Iodide Cluster Diameter (Eq. 12, Fig. 15).

Photographic Correlation with Photoluminescence Spectra. Table II describes the photographic correlation with a γAgI cluster cryogenic photoluminescence spectrum.

It is noteworthy to observe the highest obtainable speed between 10 and 30 sec of iodide addition with the

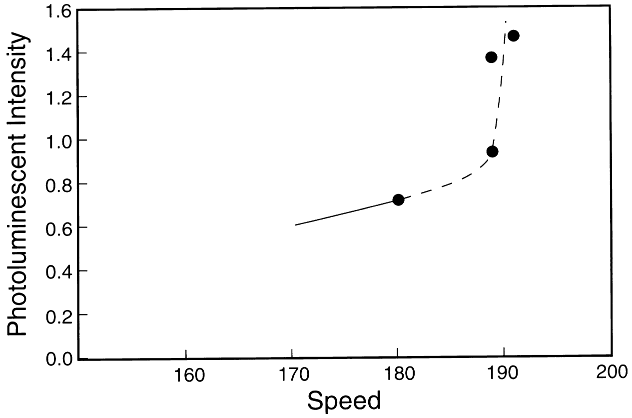

Figure 25. The correlation of the 10 K photoluminescent γAgI cluster/AgCl intensity ratio versus the photographic speed.

TABLE II. Photographic Correlation with Photoluminescent Intensity of Sample Dispersions

	Sample emulsions				
	A	B	C	D	E
Time (sec) KI addition	0	10	30	90	180
Speed	10	189	191	189	180
D-min	0.16	0.10	0.10	0.09	0.08
Toe	0.44	0.36	0.37	0.38	0.34
Emission peak (nm)					
470	0.320	0.668	0.739	0.722	0.680
500	0.240	0.458	0.475	0.720	0.888
Ratio @ 470/500 nm	1.333	1.458	1.556	1.003	0.766

available mixing geometry of the kettle. The ratio of the 470/500 nm photoluminescence bands is to normalize the emission from the γAgI cluster formation to the intrinsic AgCl grain emission or background signal.

Figure 25 shows the rapid rise of γAgI cluster/AgCl luminescent signal amplitude and the correlation to the photographic speed.

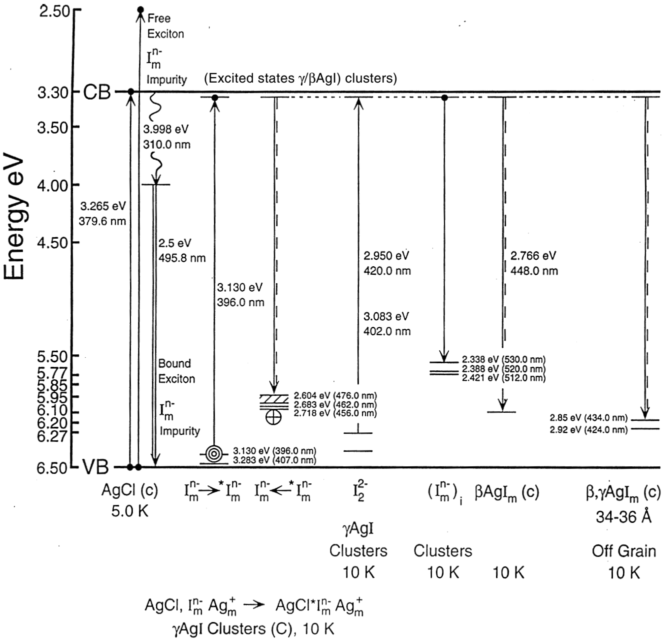

Figure 26. A summary of energy levels of γAgI, βAgI, and I_m^{n-} within the AgCl cubic lattice system (obtained from 10 K photoluminescent spectra). Reference 6(a) describes the proposed iodide ion species but not the γAgI clusters or dimers of larger I_m^{n-} clusters.

Figure 26 is a summary of energy levels of γAgI, βAgI, and I_m^{n-} within the AgCl cubic lattice system obtained from 10 K photoluminescent spectra.

Mechanisms of Iodide Luminescence. Figure 27 represents the structures and mechanisms involving the luminescent iodide centers in silver chloride competing for the conduction band electrons. The energy state diagram (a) provides a mechanism for the analysis for the photophysics, i.e., radiative and radiationless processes that correspond to electronic transitions between the

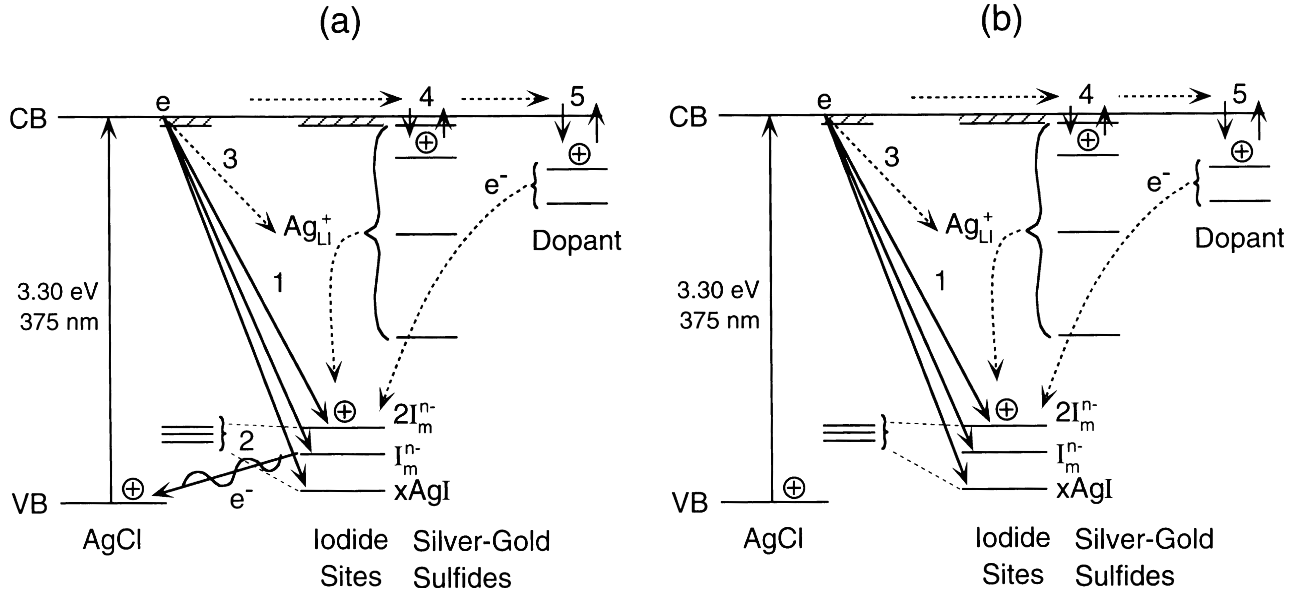

Figure 27. (a) Electronic structures and mechanisms involving the luminescent iodide centers in silver halide with introduction of Frenkel disorder. (b) Photochemical model of luminescent iodide centers with relation to Frenkel point defects. CB, conduction band; VB, valence band.

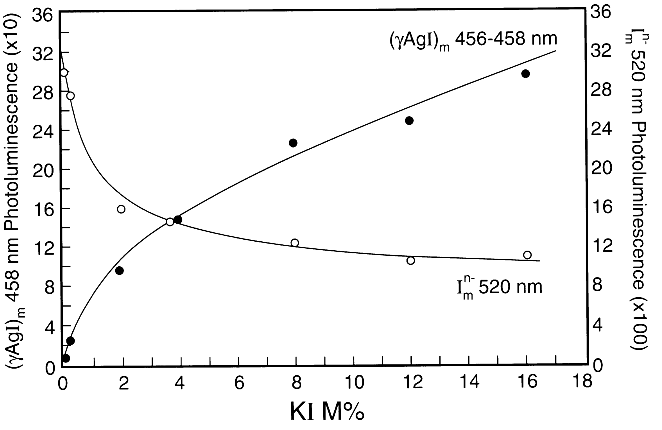

Figure 28. A plot of the steady-state photoluminescence of gAgI cluster intensity at 456 to 458 nm and the I_m^{n-} cluster intensity at 520 nm versus KI molar concentration at 10 K.

states without introducing Frenkel disorder relating to point defects; (b) relates to Frenkel disorder, including dopant compensation in both cases (a) and (b).

Figure 27(a) shows the competition for the conduction band electrons by the bound hole on the iodide sites, the LUMO of the silver–gold sulfides, and the compensated dopant species.[31] In this figure, the HOMO of the iodide species transfers an electron to the valence band hole subsequent to excitation, thus injecting a hole into the iodide sites where electron recombination site emission is detected in direct competition with the latent image formation or sulfide trapping centers and the dopant centers.[31] The limitation of this recombination mechanism is the rate of transfer of the iodide cluster HOMO electrons to the valence band hole. This rate must be greater than the rate of electron recombination with the hole at the iodide site, i.e., 2 > 1 > 3. If 1 ≥ 3, then the image formation becomes inefficient, and if 1 < 3 then the latent image formation is diminished by the ratio of the rate constants k_1/k_3. Likewise, the competition by the dopant $Cs_2[Os(NO)Cl_5]$, 78.88 molecule/grain with a concentration of 9.43×10^{-9} mole/Ag mole (5 μg/Ag mole) reduced the iodide photoluminescence of 5.00×10^{-3} mole/Ag mole by 44.96% as shown in Fig. 22(c) when using a nondopant reference of the same iodide concentration. The cross section is then assumed to be higher within the dopant. At the higher iodide concentration of 0.02 mole/Ag mole the emission quenching was 24.09%. Thus, the increased spatial separation and concentration modifications are suggested means of controlling the electron transfer between these two centers. It may then be proposed 2 > 5 > 1 > 3.

Figure 27(b) describes an alternative low-probability mechanism[32,33] relating a positive charge site for the iodide-recombination cluster emission in terms of Frenkel disorder on the halide sublattice (equal number of vacancies in the halide sublattice and in the halide interstital ions). This configuration may lead to a high-energy strained crystal arrangement due to the size of the iodide ion. The more probable mechanism would involve the defect iodide associated with the interstitial silver ion or as shown throughout this article, the γAgI quantum clusters. As shown in Fig. 27(b), the iodide clusters are competing with the conduction-band electrons subsequent to excitation in order to form the latent image center. If the latent image center quenches the iodide emission 3 > 1 and when 1 > 3, the photographic efficiency may be diminished by the ratio of k_1/k_3. The reduction of the iodide emission places the rates of the processes in the following order: 5 > 1 > 3. The controlling process relates to the product of the trapping sites and the position of the site's energy beneath the conduction band as well as the cross sections for the competing electron traps. The competing process of 4 versus 5 would be determined by the above statement.

Equilibrium of γAgI and I_m^{n-} Clusters. Figure 28 shows a plot of the relationship between the equilibrium γAgI cluster emission intensity at 456 to 458 nm with the I_m^{n-} cluster intensity at 520 nm versus KI molar concentration at 10 K. The emission intensity of the γAgI growing crystallites increase at the expense of the I_m^{n-} luminescence. This phenomenon was also viewed in the cryoscopic optical microscope.

Conclusions

1. From photoluminescence studies, I_m^{n-} acts as a recombination center in AgCl at low temperatures.

2. Heterogeneous phases exist within the cubic AgCl host lattice to provide enhanced photographic properties.
   - The γAgI nanoclusters form within the AgCl matrix with a photoluminescence intensity maximum at 455.0 nm, 2.724 eV when excited at 390.0 nm, 3.178 eV at 10 K.
   - The γAgI crystallite photoluminescence bands diminish and shift to longer wavelengths as larger clusters form due to different methods of iodide addition. The photographic parameters are not due to the chemical constituents - per se, but to the nature or structure of the γAgI crystallites within the host lattice.
   - Small clusters of βAgI are also formed and not incorporated within the host cubic lattice.
   - The correlation between γAgI nanoclusters' photoluminescence within the cubic AgCl lattice and the photographic speed parameters is demonstrated.

3. Positioning of the iodide heterogeneous phase, within the AgCl cubic host lattice, introduces changes observed by the photoluminescence and the photographic speed parameter.
   - Introduction of 0.30 M% soluble KI or 4.30 M/V% at 93% of the crystal growth provides a maximum speed position and significant change in the photoluminescence spectral band profile directly correlating with the structures of γAgI.
   - Iodide clusters are observed at longer wave lengths, 512 to 540 nm, and are assigned to 2 dimers that relate indirectly to the photographic process. The higher the 2 I_2^{n-} band intensity, the lower the γAgI band, hence a reduced photographic response.
   - The ratio of γAgI molecules/2 I_2^{n-} was calculated to be 7.46 at 0.3 M% KI and 10 K. A dynamic equilibrium appears to exist between the γAgI clusters and the 2 I_2^{n-} structures.
   - The ΔE_{act} determinations place the LUMO of the γAgI species very close to the conduction band.

4. The calculation for the diameter of a γAgI cluster allows the determination of the exciton volume and subsequently the number of unit cells and hence the number of γAgI molecules within these unit cells.

5. The dopant $Cs_2[Os(NO)Cl_5]$ in parts per billion (10^{-9} mole/Ag mole) competes favorably for the conduction

band electron as noted by the quenching of the iodide (10^{-3} mole/Ag mole) photoluminescence.▲

References

1. C. E. Mees and T. H. James, *The Theory of the Photographic Process*, Eastman Kodak Company, Rochester, NY, 1977, 4th ed., pp. 37–50.
2. G. C. Farnell, P. C. Burton, and R. Hallama, *Phil. Mag.* **41,** 157; 545 (1950).
3. F. Moser and F. Urbach, *Phys. Rev.* **106,** 852 (1957).
4. H. Kanzaki, S. Sakuraga and K. Sakamoto, *Sol. State Commun.* **9,** 999 (1971).
5. H. Kanzaki, T. Hattori and S. Sakuragi, *Phys. Chem. Sol.* 165 (1971).
6. (a) F. Moser, R. K. Ahrenkiel and S. L. Lyn, *Phys. Rev.* **161,** 897 (1967); (b) N. R. Nail, F. Moser, P. E. Goddard, and F. Urbach, *Rev. Sci. Instr.* **28,** 275 (1957); (c) W. West and V. I. Saunders, *J. Phys. Chem.* **63,** 45 (1959).
7. D. L. Dexter, *Phys. Rev.* **101,** 48 (1956).
8. G. Racah, *Phys. Rev.* **61,** 537(L) (1942).
9. M. Cardona, *Phys. Rev.* **129,** 69 (1963).
10. W. B. Fowler and D. L. Dexter, *Phys. Rev.* **128,** 2154 (1962).
11. H. Kanzaki and S. Sakuragi, *Photo. Sci. Eng.* **17,** 69 (1973).
12. S. H. Ehrlich, *J. Imaging Sci. Technol.* **39,** 97 (1995).
13. S. H. Ehrlich, *J. Imaging Sci. Technol.* **37,** 73 (1993).
14. S. H. Ehrlich, *J. Imaging Sci. Technol.* **41,** 13 (1997).
15. L. E. Brus, *J. Phys. Chem.* **90,** 2555 (1986).
16. L. E. Brus, *J. Phys. Chem.* **80,** 4403 (1984); *ibid* 79, 5566 (1983).
17. L. E. Brus, *IEEE, J. Quantum Electron* **22,** 1909 (1986).
18. A. Henglein, *Top. Current Chem.* **143,** 113 (1988).
19. A. Henglein, *Chem. Rev.* **89,** 1861 (1989).
20. H. Weller, A. Fojtik and and A. Henglein, *Chem. Phys. Lett.* **117,** 485 (1985).
21. J. Wörmer, M. Joppien, G. Zimmer, and T. Möller, *Chem. Phys. Lett.* **172,** 201 (1990).
22. Y. Wang, *Advances in Photochemistry*, Volume 19, D. C. Neckers, D. H. Volman and G. Von Bünau, Eds., Wiley Interscience, John Wiley, New York, 1995, p. 179.
23. S. H. Ehrlich, *J. Imaging Sci. Technol.* **38,** 201 (1994).
24. E. W. Washburn, Ed., *International Critical Tables of Numerical Data, Physics, Chemistry and Technology*, McGraw-Hill Book Co., New York, 1930, pp. 7, 21.
25. D. R. Lide, Ed., *CRC Handbook of Chemistry and Physics*, 71st ed., CRC Press, Boca Raton, Florida, 1990–1991, pp. 12–58, 59.
26. F. Low and D. Pines, *Phys. Rev.* **98,** 414 (1955); J. P. Spoonhower, *J. Phys. Chem. Sol.* **51,** 793 (1990).
27. M. Tsukakashi and H. Kanzaki, *J. Phys. Soc. Jpn.* **30,** 1423 (1970).
28. H. Kanzaki and S. Sakuragi, *J. Phys. Soc. Jpn.* **27,** 109 (1969).
29. W. Czaja and A. Baldereschi, *J. Phys. Colloq.; Sol. State Phys.* **12,** 405 (1979).
30. V. M. Belous, V. P. Churashov, V. V. Suvorin, F. I. Tolstobrov, and Kh. I. Shelekhov, *Shern. Mauch. I. Priklad. Fotogr. i Kinematogr.* **23,** 196 (1978).
31. S. H. Ehrlich and I. H. Leubner, *J. Imaging Sci. Technol.* **36,** 105 (1992).
32. S. Sonoike and T. Nagashima, *J. Imaging Sci.* **30,** 127 (1986).
33. S. Sonoike, *J. Imaging Sci.* **35,** 176 (1991).